Journal of Power Technologies 102 (1) (2022) 1 -- 13

Elements of supercritical CO_2 cycles—mathematical modeling and validation on available experimental data

Jarosław Milewski✉, Arkadiusz Szczęśniak, Łukasz Szablowski, Kamil Futyma, Piotr Lis, Olaf Dybiński, Marcin Wołowicz

[1]Warsaw Affiliation University, Faculty of Power and Aeronautical Engineering, Institute of Heat Engineering, 21 Nowowiejska Street, 00-665 Warsaw, Poland

✉ jaroslaw.milewski@pw.edu.pl

Abstract

This paper presents models of three elements: heat exchanger, compressor and expander dedicated to supercritical CO_2 cycles (Brayton). The models are built using Ebsilon software and validated against experimental data from available literature. Radial turbomachinery and thin plate heat exchangers were used to meet the demands of the relatively compact design of the S-CO_2 cycle elements. It seems that there are no general relationships for the turbomachinery and real characteristics need to be used for constructing the models.

Introduction

Renewable power sources, e.g., solar power [1], are highly variable in terms of output in many parts of the world, hence their development should go hand-in-hand with measures to integrate them with energy systems, e.g., integration of solar power with CCS system [2]. A very promising approach for dealing with the variability of renewable resources is involvement of large-scale energy storage. There are several areas that still have development potential in this case: liquid or compressed air energy storage [3,4], heat storage [5] or power-to-gas-to-power [6]. The latter technology uses hydrogen produced from renewable energy in various electrolysis plants [7–13]. This hydrogen can then be co-fired by gas turbines [14,15] or used in fuel cells. Due to the high efficiency and environmental friendliness, high-temperature fuel cells seem to be very future-proof energy sources (in contrast to CHP systems based on internal combustion engines) [16], hence fuel cells such as SOFC [17–30] H+SOFC [31–33] and MCFC [34–41] should be considered as methods for energy recovery from hydrogen. Due to the fact that the MCFC operating temperature (around 650°C) fits the needs of the Brayton super CO_2 cycle, these two energy sources can be connected in series (S-CO2 as a bottoming cycle) to improve the efficiency of energy conversion [42].

Work on the properties of various working media for the supercritical cycle dates back to the 1960s [43]. CO_2 has proven to be the most appropriate operating medium for several reasons. One is that CO_2 has a lower critical point pressure than water and therefore allows it to operate at a lower pressure. Another argument is that the transport and thermodynamic properties are very well known for this working medium. CO_2 is readily available, cheap and non-toxic. The thermodynamic cycle based on supercritical carbon dioxide has many advantageous features such as: high power in relation to the flow of the working medium, high efficiency (even 55% in ideal conditions), no cavitation and corrosion of the turbine blades. Almost 40 years later Dostal started researching supercritical carbon dioxide [44]. He dealt with the analysis of supercritical CO_2 systems for applications in nuclear power (for advanced nuclear reactors). He conducted an analysis of individual elements of the system as well as entire systems for this type of application. This was followed by a report that predicted the cost of supercritical CO_2 systems operating on the Brayton cycle for use in fourth generation nuclear reactors [45]. The two publications above gave rise to a series of other studies on supercritical carbon dioxide systems.

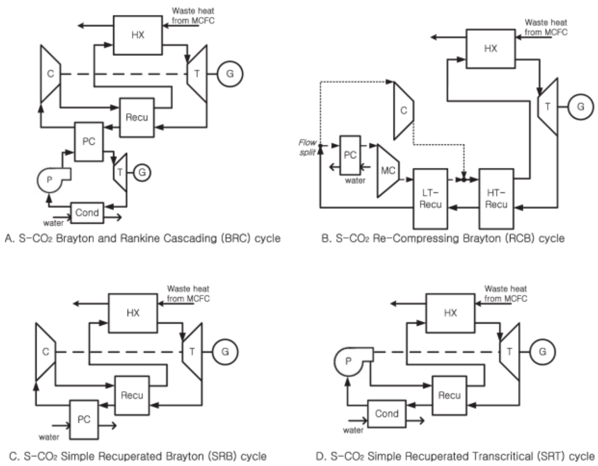

Fig. 1 Various sCO_2 cycle layouts [42]

Different S-CO_2 cycles have been compared by Bae et al. (Fig. 1). As a result of this analysis, it was found that all cycles using super CO_2 in the Brayton cycle had better performance than the cycles using air as the working medium. The systems from Fig. 1 b, a and d contributed to the increase in the net efficiency of the entire hybrid system (MCFC - S-CO_2 system) by more than 10% in relation to the MCFC system without waste heat recovery [42]. The aim our paper is to develop models of the main elements of S-CO2 cycles as they are presented in Fig. 1. The following elements can be found in each system:

1. Compressor
2. Expander (turbine)
3. Heat Exchanger
4. Pump (in Rankine cycles)

Due to the relatively small sizes of the supercritical cycles, the turbomachinery used is also relatively small and often based on radial constructions (Fig. 6 and Fig. 11). The modeling of expanders and compressors is mainly based on energy balance equations, assuming constant efficiency; see [46]. More advanced studies like [47] take into consideration models which use mean-line flow analysis performance prediction for map of the off-design parameters. This approach involves four-dimensional parameter tables (rotational speed of the shaft, pressure, mass flow rate, and inlet temperature). To determine the output parameters (pressure and temperature) the input parameters are interpolated. Generating four-dimensional maps takes a lot of work, but works reasonably well. In fact, maps taken from this source were used in the present study.

For design purposes a detailed CFD can be used to model the CO_2 flow between turbomachinery blades, as shown in [48–50]; or more simply the similarity concept can be used [51]. Commercial software is available for estimating the main dimensions of the turbomachinery [52]. [53] shows a new method of modeling performance maps for stages of centrifugal compressor. Four dimensionless parameters were used to characterize the performance at design point. Using this new approach, the entire performance map is based on these four parameters using algebraic equations that do not require exact knowledge of the geometry of the device.

A 1-d model for the design and evaluation of carbon dioxide compressor parameters is shown in [54]. A centrifugal compressor operating at high rotational speeds and mounted on foil gas bearings was modeled. The model was validated against data of Sandia Laboratories of a 50 kW compressor total efficiency.

Heat exchangers in S-CO_2 cycles operate at relatively low temperatures and high pressures. Serrano et al. [55] a methodology is presented which consists in designing heat exchangers in appropriate sizes for use in the Brayton cycle for supercritical CO_2. The working media on both sides of the heat exchanger (which cannot be too large) in such a cycle are characterized by a large pressure difference, therefore the use of PCHE (Printed Circuit Heat Exchangers) is suggested. Various empirical relationships between the Nusselt number and pressure drop were assessed there. The construction of a low-temperature regenerative heat exchanger and a pre-cooler were also tested using CFD methods due to the fact that they operate at near critical point of CO_2. In [56] the forced convection in a semicircular, printed circuit heat exchanger was modeled and experimentally validated for supercritical carbon dioxide as working medium and similar work was presented by [57]. For heat transfer in supercritical CO_2 during forced convection, a physically improved semi-empirical correlation with significantly improved predictions was proposed in [58].

Theory

Heat exchanger

The task of the heat exchanger is to transfer heat from the medium with a higher temperature to the medium with a lower temperature. In S-CO_2 cycles there are as many as three points in the cycle where a heat exchange process is employed (heat input, heat rejection and recuperation), hence heat exchangers play a critical role in cycle design.

Two types of losses dominate in the description of the heat exchanger model. The first one concerns the process of heat exchange between two fluids and is related to a specific temperature difference (ΔT), which is caused by a limited heat transfer area. The magnitude of temperature difference losses is usually assessed by using a concept of effectiveness defined as:

$$\epsilon_R = \frac{Q}{Q_{\max}}$$

In this formula, in the numerator is the heat actually exchanged in the heat exchanger and in the denominator – the maximum theoretically exchangeable heat if the heat transfer area were infinite.

Besides the ΔT losses, there are frictional pressure drops ΔP in the exchanger channels. These losses depend on other parameters, namely the type of flow (laminar or turbulent) and the geometry of the channels. The total pressure drop is obtained by taking into account all the existing contributions:

$$\Delta p = \Delta p_i + \Delta p_c + \Delta p_a + \Delta p_e$$

where:

Δp_i —entrance loss; Δp_c —core loss (friction term); Δp_a —core loss (acceleration/decelaration term); Δp_e—exit loss [59].

Pressure losses generally increase as the heat transfer area increases. Therefore, the pressure loss (ΔP) and the temperature difference (ΔT) in the case of a heat exchanger are inversely related. Increasing heat transfer is associated with an increase in the heat exchange surface, which increases the price of the heat exchanger and greater energy needs related to overcoming flow resistance. As a result, it is difficult to determine whether certain modifications to the heat exchanger structure will positively affect its performance [60].

Line connections	
1	Primary side inlet (cold stream, inside tubes)
2	Primary side outlet (cold stream, inside tubes)
3	Secondary side inlet (hot stream, outside tubes)
4	Secondary side outlet (hot stream, outside tubes)
5	(K*F)-controlling inlet

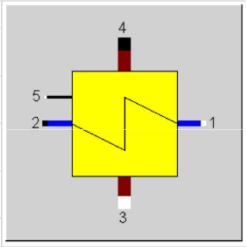

Fig. 2 Specifications of a model heat exchanger in the software used

Fig. 2 shows the heat exchanger model in the EBSILON software. The model contains four connections: inlet and outlet streams for two sides of the heat exchanger and additionally a controlling connection.

Expander

In general, a turbine is a rotating machine which receives energy from the working medium during the process of its expansion (with a simultaneous decrease in the enthalpy of the medium) and converts it into mechanical energy received on the shaft. It is assumed that the expansion process, which happens during turbine work, is an adiabatic not isentropic process. Thus, a definition of efficiency has to be introduced:

$$\eta_T = \frac{h_3 - h_4}{h_{3,s} - h_4} = \frac{\Delta h}{\Delta h_s}$$

where letters denoted by index s stand for ideal values that would occur in the isentropic expansion process. h_3 and h_4 are specific enthalpy values before and after the turbine respectively. Reduced turbine efficiency reduces the thermal efficiency of a cycle and the total work output. However, turbine imperfections are not as detrimental to total cycle work output as those of a compressor, since the heat produced in the dissipation process is transferred to the working fluid and thus can be utilized by subsequent turbine stages.

The General Expander component (see Fig. 3) converts thermal/potential energy of a process vapor into mechanical energy on a shaft. It can be applied to water (incompressible flow, hydraulic turbine), steam or any gases as defined by stream type: gas, flue gas, universal fluid, and 2-phase vapor/liquid (compressible flow, turbo machinery). As such it is a most versatile component in EBSILON when modeling energy conversion by means of expansion of a process stream. The General Expander represents a single expansion stage, a stage group or a complete expansion section of the modeled equipment.

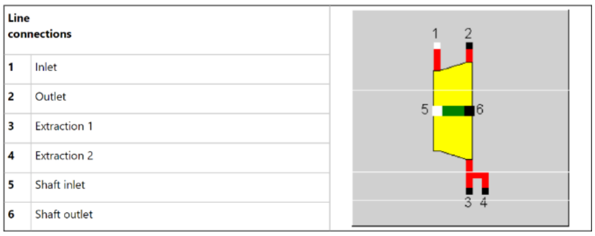

Fig. 3 A view of the model topological icon of expander in the used software

The expander model is shown in Fig. 3; the model has inlet and outlet streams as well as extractions. Two energy streams can be connected to the model.

Compressor

A compressor is a device that, using mechanical energy, can efficiently raise the pressure in a compressible medium (as opposed to a pump that increases pressure in an incompressible medium). Since liquids are not compressible or poorly compressible, there is no substantial change of liquid volume during pump work.

Under ideal conditions, the transformation taking place in the compressor is isentropic. In the actual process, there is an increase in entropy. This deviation from ideal performance can be measured using isentropic efficiency, which can be described as follows:

$$\eta_{C(P)} = \frac{h_{1,s} - h_0}{h_1 - h_0} = \frac{h_s}{h}$$

Isentropic efficiency depends on both internal and external factors. Airfoil design exerts a critical influence on compressor performance, but fluid medium composition and inlet conditions may also affect compressor efficiency.

Most of the rotary machines operating in the Brayton cycle use working agents whose properties are close to the ideal gas. S-CO_2 cycle compressors operate near critical point, thus a real gas model has to be used.

The model compressor was implemented in Ebsilon Professional by using the “compressor” component . In general, this component is used to simulate an increase in pressure of the medium.

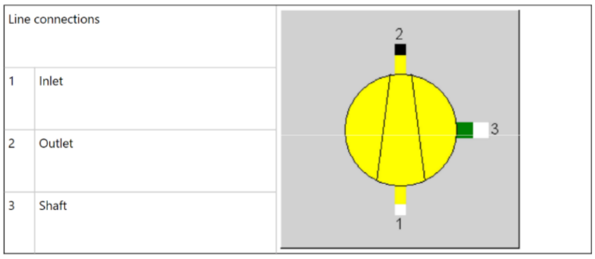

Fig. 4 Compressor component

As shown in Fig. 4, the model of a compressor requires two material streams (inlet and outlet) and one energy stream (shaft power). In S-CO_2 cycles we do not assume any cooling system for the compressor (intersection cooling), thus the model seems appropriate for the given task.

Calculation mode (design / off-design)	FMODE	GLOBAL : 0	
Specification of enthalpies and power	FSPECH	Efficiency charline used : 0	
Validation of isentropic efficiency	FVALETAI	ETAIN used without validation : 0	
Isentropic efficiency (nominal)	ETAIN	0.85	-
Index for pseudo measurement point	IPS		
Usage of ADAPT / EADAPT	FADAPT	Not used and not evaluated : 0	
Adaptation function	EADAPT		
Mechanical efficiency (nominal)	ETAMN	0.99	-
Mechanical loss (constant fraction)	QLOSSM	0	kW
(Deprecated) type of charline	FCHR		
Mass flow (nominal)	M1N	0.3	kg/s

Fig. 5 List of required parameters for Ebsilon

The selected component requires the connection of three streams: inlet gas, outlet gas and shaft (power) and requires definitions of isentropic and mechanical efficiency. The list of required input parameters is displayed in Fig. 5.

Validation of the used models

CO_2 compressor

The model CO_2 compressor is validated with experimental data provided by Sandia National

Laboratories [48]. The compressor wheel is shown in Fig. 6.

Fig. 6 CO_2 compressor at Sandia National Laboratories [48]

Fig. 7 shows the image from the data acquisition and control system. It illustrates the T-S diagram of S-CO_2 where the working medium parameters at specific locations are plotted for the experiment during which the shaft rotational speed was changed from 10,000 rpm to 65,000 rpm. Green points indicates the outlet parameters and red indicates the compressor inlet parameters on the T-S diagram.

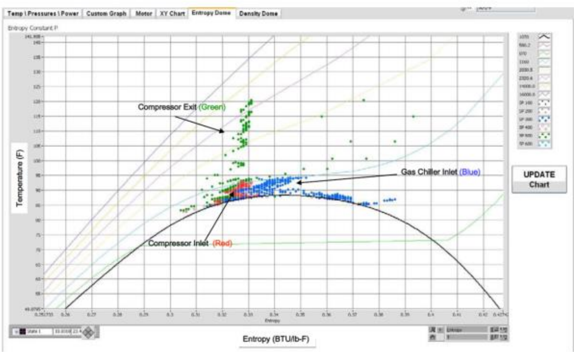

Fig. 7 Screenshot obtained from the control system of the Sandia S-CO_2 test bench for the compressor. Here we can see the operating parameters of the working medium at the inlet (red) and at the outlet of the compressor (green) on the T-S diagram [47]

Based on the experimental data from Sandia National Laboratories, the performance map of the compressor was created – Fig. 7. The efficiency was obtained using the measured power of the motor controller minus the losses of windage and the power losses of the pump vane. The latter were estimated as 17% of the windage losses. In addition, the authors of [47] proposed a model of the examined compressor and its performance compared with experimental data, which are displayed in the performance map in Fig. 8.

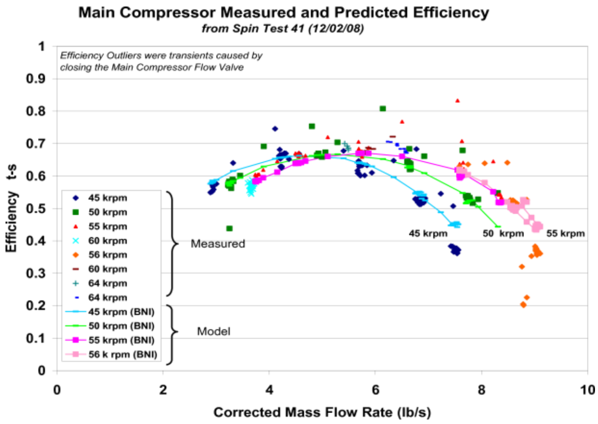

Fig. 8 Comparison of the actual and calculated by the model efficiency of the main compressor in the Sandia National Laboratories S-CO_2 test bench. The diagram shows the compressor efficiency vs corrected mass flow rate [47]

Data used for validation are taken from the High Speed Spin Test (75000,00 rpm). Compressor performance during this test is displayed in Table 1. The simulation results of the compressor, which was tested at Sandia National Laboratories, are shown in Fig. 9.

Table 1 Comparison of experimental data and simulation results

	Test data [63]	Validation
Pressure at the inlet, bar	76.90	76.90
Temperature at the inlet, K	305.3	305.3
Pressure at the outlet, bar	139.84	139.84
Temperature at the outlet, K	324.66	324.151
Mass flow, kg/s	3.53	3.53
RPM, rev/min	75000	—
Efficiency, %	75.2	75.2

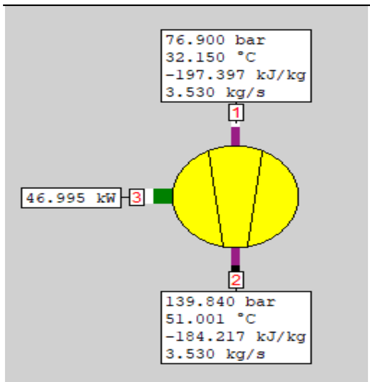

Fig. 9 Simulation results of compressor

CO_2 expander

The model of CO_2 expander is verified with the main compressor turbine, which is installed in test loop at Sandia National Laboratories [48]. The examined turbine operates in a split-flow recompression Brayton cycle – denoted as Turb-1 in Fig. 10.

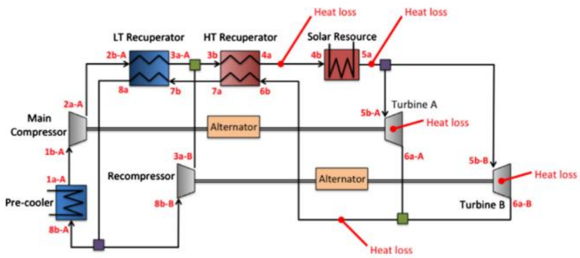

Fig. 10 Scheme of split-flow recompression Brayton cycle [61]

The design of the radial turbine wheel (see Fig. 11) was developed by BNI. It is made of Inconel 718 because of its resistance to stress and high temperatures. The turbine performance map is shown in Fig. 12, where the nominal working conditions are marked with a red diamond.

Fig. 11 Wheel of main compressor turbine

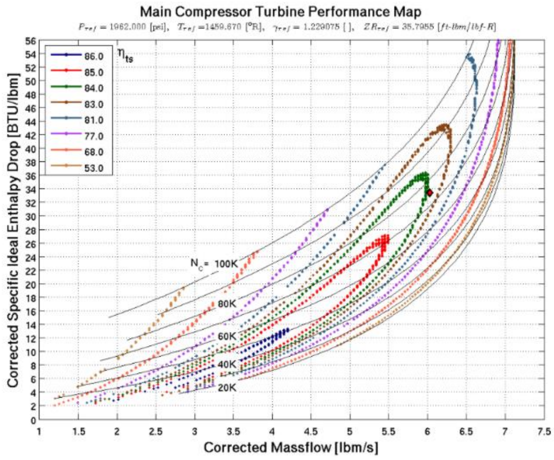

Fig. 12 Performance map of main compressor turbine [65]

Data used for validation are taken from the main compressor CO_2 turbine, which was tested at Sandia National Laboratories. State points measured at steady operation and calculated values are displayed in Table 2. The simulation results of the main compressor turbine, which was tested at Sandia National Laboratories, are shown in Fig. 12.

Table 2 Comparison of experimental data and simulation results

	Test data [61]	Validation
Pressure at the inlet, kPa	9893.7	9893.7

Inlet temperature, °C	390	390
Outlet pressure, bar	7938.4	7938.4
Temperature at the outlet, °C	368.9	367.3
Mass flow, kg/s	1.741	1.741
Efficiency, %	86	86

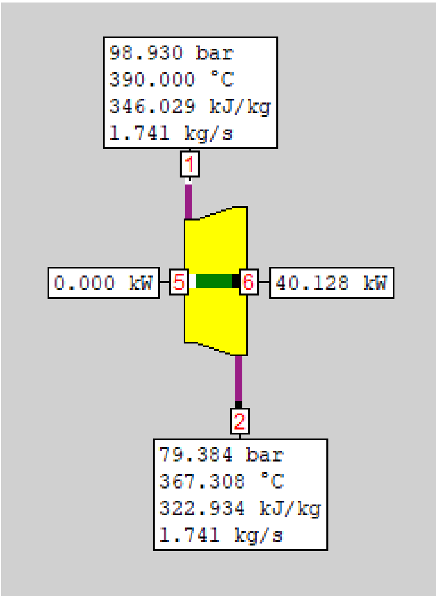

Fig. 13 Simulation results of CO_2 expander

Heat Exchanger

The mathematical model of the heat exchanger is verified with experimental data published by [61], where it is was installed in a split-flow Brayton test loop at Sandia National Laboratories [62]. The layout of the system is presented in Fig. 10. The high temperature regenerative heat exchanger is denoted as HT-recuperator. The examined device is a High-Temperature PCHE (printed circuit heat exchanger) recuperator manufactured by Heatric. A photo of this device is shown in Fig. 14.

Fig. 14 S-CO_2 high temperature PCHE recuperator at Sandia National Laboratories [63]

The material used for the construction of the heat exchanger is 316 steel and its design power is 2.3 MW for a flow of 5.7 kg / s and an inlet temperature of 755 K on the hot side and a maximum working pressure of 17.2 MPa [62]. The approximate dimensions of the HT Recuperator are shown in Table 3.

Table 3 Approximate Dimensions of the HT PCHE Recuperator installed in test loop at Sandia National Laboratories

Property	Value
HT Recuperator	
Channel Width	1.27 mm (0.05 in.)
Channel Depth	0.77 mm (0.0303 in.)
Plate Depth	1.69 mm (0.0665 in.)
Flow Area per Channel	0.768 mm^2 (0.00119 in.^{2})
Hydraulic Diameter (Dh)	1.0607 mm (0.0418 in.)
Core	
Height	0.296 m (11.65 in.)
Length	0.996 m (39.21 in.)
Width	0.512 m (20.16 in.)
Heat Transfer Area	43 m^2 (462.80 ft^2)
Core Mass	1410 kg (3108 lbm)

The model presented in this article was verified on the basis of experimental data from [61]. The data were collected after 7600s, i.e. at a time of steady power generation [61]. The measurements were taken at the following points denoted in Fig. 10, i.e.:

- point 3b - cold side temperature & pressure measurement,
- point 4a - hot side temperature & pressure measurement,
- point 6b - hot side temperature & pressure measurement,
- point 7a - cold side temperature & pressure measurement,
- points 6a-A & 6a-B - mass flow measurement,
- points 2a-A & 3a-B - mass flow measurement.

The simulation results of HT Recuperator are displayed in Fig. 15. The comparison of the experimental data with the modeling results is shown in Table 4.

Table 4 Comparison of experimental data and results of simulation for Heat Exchanger

	Test data [61]	Validation
Hot side temperature (4a), °C	331.7	331.7
Cold side temperature (3b), °C	58.7	58.7
Hot side temperature (6b), °C	366.3	366.3
Cold side temperature (7a), °C	67.0	69.902
Pressure drop across flow 3b - 4a, kPa	100	100
Pressure drop across flow 6b - 7a, kPa	138.7	138.7
Mass flow in line 3b - 4a, kg/s	3.483	3.483
Mass flow in line 6b - 7a, kg/s	3.428	3.428

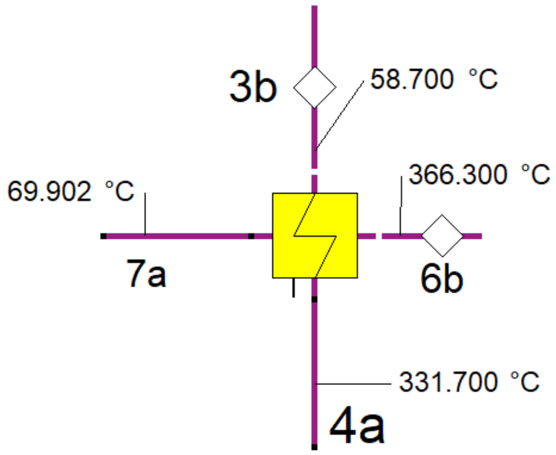

Fig. 15 Simulation results of Heat Exchanger—model implemented in Ebsilon professional simulation software

Discussion and conclusions

We built and validated three elements: expander, compressor, and heat exchanger dedicated to modeling S-CO_2 cycles. The models were validated based on available experimental data.

Table 5 Comparison of the models created

Property	CO_2 compressor	CO_2 expander	Heat exchanger
Power/Heat range, kW	45	40	1,5
Temperature range, °C	32 .. 51	370 .. 390	60 .. 370
Pressure range, bar	77 .. 140	80 .. 100	–
Pressure ratio	2	1.25	–
Efficiency/ effectiveness, %	75	86	95
Modeling error, %	3	7	1

The models were simulated in various power, temperature and pressure ranges (see Table 5). The power ranges of the turbomachinery are not very well fitted to the heat exchanger size. The heat flow transferred in the heat exchanger is 33.3 to 37.5 times greater than in the turbomachinery. Modeling of heat exchangers does not require specific characteristics, thus the model can be readily used for lower heat ranges, whereas for the turbomachinery we used specific characteristics of real devices. The temperature range of work of the heat exchanger lies within the range of the turbomachinery, leaving a difference of around 20-30°C for the heat transfer process to happen. The compressor works at between 77 and 140 bar, giving a compression ratio close to 2, while expanding pressure changes from 100 to 80 bar, resulting in a pressure ratio of 1.25. The efficiencies of the presented compressor, expander and heat exchanger are 75%, 86% and 95% respectively. The created models deliver results with error below 10%, which seems reasonable.

The paper presents the models of basic elements of S-CO_2 cycles. We built the following models: heat exchanger, CO_2 compressor and CO_2 expander. The models were validated based on real characteristics taken from literature references. The characteristics were entered into Ebsilon software. There are small deviations between the calculated values and those provided by experiments.

Due to the relatively small sizes of the turbomachinery used in S-CO_2 cycles, it is not possible to use the Flugel–Stodola equation [64] for modeling turbine flow parameters; instead, real characteristics must be used.

Since all the models were created in the same numerical environment, they can be used for building various, mutually-coherent systems which can be used for analysis of the system layout

Acknowledgments

The work is financed by the National Science Center, Poland, 2015/19/D/ST8/02780

References

[1] Siddiqui O, Dincer I. Analysis and performance assessment of a new solar-based multigeneration system integrated with ammonia fuel cell and solid oxide fuel cell-gas turbine combined cycle. J Power Sources 2017;370:138–54. https://doi.org/10.1016/j.jpowsour.2017.10.008.

[2] Bonaventura D, Chacartegui R, Valverde JM, Becerra JA, Ortiz C, Lizana J. Dry carbonate process for {CO} 2 capture and storage: Integration with solar thermal power. Renew & Sustain ENERGY Rev 2018;82:1796–812. https://doi.org/10.1016/j.rser.2017.06.061.

[3] Krawczyk P, Szabłowski Ł, Karellas S, Kakaras E, Badyda K. Comparative thermodynamic analysis of compressed air and liquid air energy storage systems. Energy 2018;142:46–54. https://doi.org/10.1016/j.energy.2017.07.078.

[4] Szablowski L, Krawczyk P, Badyda K, Karellas S, Kakaras E, Bujalski W. Energy and exergy analysis of adiabatic compressed air energy storage system. Energy 2017;138:12–8. https://doi.org/10.1016/j.energy.2017.07.055.

[5] MichałLeśko, Bujalski W. Modeling of District Heating Networks for the Purpose of Operational Optimization with Thermal Energy Storage. Arch Thermodyn 2017;38:139–63. https://doi.org/10.1515/aoter-2017-0029.

[6] Kotowicz J, Bartela L, Dubiel-Jurgas K. Analysis of energy storage system with distributed hydrogen production and gas turbine. Arch Thermodyn 2017;38:65–87. https://doi.org/10.1515/aoter-2017-0025.

[7] Clúa JGG, Mantz RJ, Battista H De. Optimal sizing of a grid-assisted wind-hydrogen system. Energy

Convers Manag 2018;166:402–8. https://doi.org/10.1016/j.enconman.2018.04.047.

[8] Nadar A, Banerjee AM, Pai MR, Pai R V, Meena SS, Tewari R, et al. Catalytic properties of dispersed iron oxides Fe2O3/MO2 (M = Zr, Ce, Ti and Si) for sulfuric acid decomposition reaction: Role of support. Int J Hydrogen Energy 2018;43:37–52. https://doi.org/10.1016/j.ijhydene.2017.10.163.

[9] Senseni AZ, Meshkani F, Fattahi SMS, Rezaei M. A theoretical and experimental study of glycerol steam reforming over Rh/MgAl2O4 catalysts. ENERGY Convers Manag 2017;154:127–37. https://doi.org/10.1016/j.enconman.2017.10.033.

[10] Fukuzumi S, Lee Y-M, Nam W. Fuel Production from Seawater and Fuel Cells Using Seawater. ChemSusChem 2017;10:4264–76. https://doi.org/10.1002/cssc.201701381.

[11] Chen Y, Mojica F, Li G, Chuang P-YA. Experimental study and analytical modeling of an alkaline water electrolysis cell. Int J ENERGY Res 2017;41:2365–73. https://doi.org/10.1002/er.3806.

[12] Zhang C, Liu Q, Wu Q, Zheng Y, Zhou J, Tu Z, et al. Modelling of solid oxide electrolyser cell using extreme learning machine. Electrochim Acta 2017;251:137–44. https://doi.org/10.1016/j.electacta.2017.08.113.

[13] Olivier P, Bourasseau C, Bouamama PB. Low-temperature electrolysis system modelling: A review. Renew Sustain ENERGY Rev 2017;78:280–300. https://doi.org/10.1016/j.rser.2017.03.099.

[14] Mostowy M, Szablowski L. Comparison of the Brayton-Brayton Cycle with the Brayton-Diesel Cycle. J POWER Technol 2018;98:97–105.

[15] Zhuang Q, Geddis P, Runstedtler A, Bruce C, Clements B, Bruce C. An integrated natural gas power cycle using hydrogen and carbon fuel cells. FUEL 2017;209:76–84. https://doi.org/10.1016/j.fuel.2017.07.080.

[16] Carlucci AP, de Monte V, de Risi A, Strafella L. Benefits of Enabling Technologies for the ICE and Sharing Strategies in a CHP System for Residential Applications. J ENERGY Eng 2017;143. https://doi.org/10.1061/(ASCE)EY.1943-7897.0000434.

[17] Kupecki J, Motylinski K. Analysis of operation of a micro-cogenerator with two solid oxide fuel cells stacks for maintaining neutral water balance. Energy 2018;152:888–95. https://doi.org/10.1016/j.energy.2018.04.015.

[18] Prokop TA, Berent K, Iwai H, Szmyd JS, Brus G. A three-dimensional heterogeneity analysis of electrochemical energy conversion in {SOFC} anodes using electron nanotomography and mathematical modeling. Int J Hydrogen Energy 2018;43:10016–30. https://doi.org/10.1016/j.ijhydene.2018.04.023.

[19] Pianko-Oprych P, Hosseini SM. Dynamic Analysis of Load Operations of Two-Stage {SOFC} Stacks Power Generation System. ENERGIES 2017;10:2103. https://doi.org/10.3390/en10122103.

[20] Kupecki J, Motylinski K, Skrzypkiewicz M, Wierzbicki M, Naumovich Y. Preliminary electrochemical characterization of anode supported solid oxide cell (AS-SOC) produced in the Institute of Power Engineering operated in electrolysis mode (SOEC). Arch Thermodyn 2017;38:53–63. https://doi.org/10.1515/aoter-2017-0024.

[21] Zheng Y, Luo Y, Shi Y, Cai N. Dynamic Processes of Mode Switching in Reversible Solid Oxide Fuel Cells. J ENERGY Eng 2017;143. https://doi.org/10.1061/(ASCE)EY.1943-7897.0000482.

[22] Barelli L, Bidini G, Cinti G, Ottaviano A. Study of SOFC-SOE transition on a RSOFC stack. Int J Hydrogen Energy 2017;42:26037–47. https://doi.org/10.1016/j.ijhydene.2017.08.159.

[23] Genc O, Toros S, Timurkutluk B. Geometric optimization of an ejector for a 4~{kW} {SOFC} system with anode off-gas recycle. Int J Hydrogen Energy 2018;43:9413–22. https://doi.org/10.1016/j.ijhydene.2018.03.213.

[24] Azizi MA, Brouwer J. Progress in solid oxide fuel cell-gas turbine hybrid power systems: System design and analysis, transient operation, controls and optimization. Appl Energy 2018;215:237–89. https://doi.org/10.1016/j.apenergy.2018.01.098.

[25] Lorenzo G De, Fragiacomo P. Electrical and thermal analysis of an intermediate temperature {IIR}-{SOFC} system fed by biogas. Energy Sci {&} Eng 2018;6:60–72. https://doi.org/10.1002/ese3.187.

[26] Ferrel-Alvarez AC, Dominguez-Crespo MA, Cong H, Torres-Huerta AM, Brachetti-Sibaja SB, la Cruz W. Synthesis and surface characterization of the La0.7-xPrxCa0.3MnO3 (LPCM) perovskite by a non-conventional microwave irradiation method. J Alloys Compd 2018;735:1750–8. https://doi.org/10.1016/j.jallcom.2017.11.306.

[27] Abdalla AM, Hossain S, Azad AT, Petra PMI, Begum F, Eriksson SG, et al. Nanomaterials for solid oxide fuel cells: A review. Renew Sustain ENERGY Rev 2018;82:353–68. https://doi.org/10.1016/j.rser.2017.09.046.

[28] Peksen M. Safe heating-up of a full scale {SOFC} system using 3D multiphysics modelling optimisation. Int J Hydrogen Energy 2018;43:354–62. https://doi.org/10.1016/j.ijhydene.2017.11.026.

[29] Badur J, Lemanski M, Kowalczyk T, Pawel Z, Kornet S. VERIFICATION OF ZERO-DIMENSIONAL MODEL OF SOFC WITH INTERNAL FUEL REFORMING FOR COMPLEX HYBRID ENERGY CYCLES. Chem Process Eng Chem I Proces 2018;39:113–28. https://doi.org/10.24425/119103.

[30] Dillig M, Plankenbuehler T, Karl J. Thermal effects of planar high temperature heat pipes in solid oxide cell stacks operated with internal methane reforming. J Power Sources 2018;373:139–49. https://doi.org/10.1016/j.jpowsour.2017.11.007.

[31] Dzierzgowski K, Wachowski S, Gojtowska W, Lewandowska I, Jasinski P, Gazda M, et al. Praseodymium substituted lanthanum orthoniobate: Electrical and structural properties. Ceram Int 2018;44:8210–5. https://doi.org/10.1016/j.ceramint.2018.01.270.

[32] Danilov NA, Tarutin AP, Lyagaeva JG, Pikalova EY, Murashkina AA, Medvedev DA, et al. Affinity of {YBaCo} 4 O 7+$\updelta$ -based layered cobaltites with protonic conductors of cerate-zirconate family. Ceram Int 2017;43:15418–23. https://doi.org/10.1016/j.ceramint.2017.08.083.

[33] Lyagaeva J, Vdovin G, Hakimova L, Medvedev D, Demin A, Tsiakaras P. BaCe0.5Zr0.3Y0.2-xYbxO3-delta proton-conducting electrolytes for intermediate-temperature solid oxide fuel cells. Electrochim Acta 2017;251:554–61. https://doi.org/10.1016/j.electacta.2017.08.149.

[34] Davoodi AH, Pishvaie MR. Plant-Wide Control of an Integrated Molten Carbonate Fuel Cell Plant. J Electrochem Energy Convers Storage 2018;15:21005. https://doi.org/10.1115/1.4039043.

[35] Chakravorty J, Sharma G, Bhatia V. Analysis of a DVR with Molten Carbonate Fuel Cell and Fuzzy Logic Control. Eng Technol Appl Sci Res 2018;8:2673–9.

[36] Jienkulsawad P, Saebea D, Patcharavorachot Y, Kheawhom S, Arpornwichanop A. Analysis of a solid oxide fuel cell and a molten carbonate fuel cell integrated system with different configurations. Int J Hydrogen Energy 2018;43:932–42. https://doi.org/10.1016/j.ijhydene.2017.10.168.

[37] Wu M, Zhang H, Liao T. Performance assessment of an integrated molten carbonate fuel cell-thermoelectric devices hybrid system for combined power and cooling purposes. Int J Hydrogen Energy 2017;42:30156–65. https://doi.org/10.1016/j.ijhydene.2017.10.114.

[38] Accardo G, Frattini D, Yoon SP, Ham HC, Nam SW. Performance and properties of anodes reinforced with metal oxide nanoparticles for molten carbonate fuel cells. J Power Sources 2017;370:52–60. https://doi.org/10.1016/j.jpowsour.2017.10.015.

[39] Cheon Y, Lee D, Lee I-B, Sung SW. A new {PID} auto-tuning strategy with operational optimization for {MCFC} systems. 2013 9th Asian Control Conf., IEEE; 2013. https://doi.org/10.1109/ascc.2013.6606304.

[40] Samanta S, Ghosh S. Techno-economic assessment of a repowering scheme for a coal fired power plant through upstream integration of SOFC and downstream integration of MCFC. Int J Greenh GAS Control 2017;64:234–45. https://doi.org/10.1016/j.ijggc.2017.07.020.

[41] Czelej K, Cwieka K, Colmenares JC, Kurzydlowski KJ. Atomistic insight into the electrode reaction mechanism of the cathode in molten carbonate fuel cells. J Mater Chem A 2017;5:13763–8. https://doi.org/10.1039/c7ta02011b.

[42] Bae SJ, Ahn Y, Lee J, Lee JI. Various supercritical carbon dioxide cycle layouts study for molten carbonate fuel cell application. J Power Sources 2014;270:608–18. https://doi.org/10.1016/j.jpowsour.2014.07.121.

[43] Feher EG. The supercritical thermodynamic power cycle. Energy Convers 1968;8:85–90. https://doi.org/http://dx.doi.org/10.1016/0013-7480(68)90105-8.

[44] Dostal V, Driscoll MJ, Hejzar P. A Supercritical Carbon Dioxide Cycle for Next Generation Nuclear Reactors. Adv Nucl Power Technol Progr 2004.

[45] Driscoll MJ. Supercritical CO2 Plant Cost Assessment 2004.

[46] Dostal V, Driscoll MJ, Hejzlar P. A supercritical carbon dioxide cycle for next generation nuclear reactors. Massachusetts Institute of Technology, Department of Nuclear Engineering, 2004.

[47] Pickard SAWRFRMEVGERPS. Operation and Analysis of a Supercritical CO2 Brayton Cycle. SANDIA Rep 2010.

[48] Pecnik Rene; Colonna P. Accurate CFD Analysis of a Radial Compressor Operating with Supercritical CO2. Supercrit. CO2 Power Cycle Symp., 2011.

[49] Schmitt J, Amos D, Custer C, Willis R, Kapat J. Study of A Supercritical CO2 Turbine with TIT fo 1350K for Brayton Cycle with 100MW class output: Aerodynamic analysis of Stage 1 Vane. 4th Int Symp - Supercrit CO2 Power Cycles 2014.

[50] Liu Z, Luo W, Zhao Q, Zhao W, Xu J. Preliminary Design and Model Assessment of a Supercritical {CO}2 Compressor. Appl Sci 2018;8:595. https://doi.org/10.3390/app8040595.

[51] Zhao Q, Mecheri M, Neveux T, Privat R, Jaubert J-N. Selection of a Proper Equation of State for the Modeling of a Supercritical CO2 Brayton Cycle: Consequences on the Process Design. Ind Eng Chem Res 2017;56:6841–53.

[52] Nassar A, Moroz L, Burlaka M, Pagur P, Govoruschenko Y. Designing Supercritical CO2 Power Plants using an Integrated System. Power-Gen India Cent Asia 201AD.

[53] Casey M, Robinson C. A Method to Estimate the Performance Map of a Centrifugal Compressor Stage. J Turbomach 2012;135:21034. https://doi.org/10.1115/1.4006590.

[54] Kus B, Nekså P. Development of one-dimensional model for initial design and evaluation of oil-free Co2 turbo-compressor. Int J Refrig 2013;36:2079–90. https://doi.org/10.1016/j.ijrefrig.2013.05.009.

[55] Serrano IP, Cantizano A, Linares JI, Moratilla BY. Modeling and sizing of the heat exchangers of a new supercritical {CO}2 Brayton power cycle for energy conversion for fusion reactors. Fusion Eng Des 2014;89:1905–8. https://doi.org/10.1016/j.fusengdes.2014.04.039.

[56] Li H, Zhang Y, Zhang L, Yao M, Kruizenga A, Anderson M. {PDF}-based modeling on the turbulent

convection heat transfer of supercritical {CO} 2 in the printed circuit heat exchangers for the supercritical {CO} 2 Brayton cycle. Int J Heat Mass Transf 2016;98:204–18. https://doi.org/10.1016/j.ijheatmasstransfer.2016.03.001.

[57] Cui X, Guo J, Huai X, Cheng K, Zhang H, Xiang M. Numerical study on novel airfoil fins for printed circuit heat exchanger using supercritical {CO} 2. Int J Heat Mass Transf 2018;121:354–66. https://doi.org/10.1016/j.ijheatmasstransfer.2018.01.015.

[58] Meshram A, Jaiswal AK, Khivsara SD, Ortega JD, Ho C, Bapat R, et al. Modeling and analysis of a printed circuit heat exchanger for supercritical {CO} 2 power cycle applications. Appl Therm Eng 2016;109:861–70. https://doi.org/10.1016/j.applthermaleng.2016.05.033.

[59] Muzychka YS. Constructal multi-scale design of compact micro-tube heat sinks and heat exchangers. Int J Therm Sci 2007;46:245–52. https://doi.org/10.1016/j.ijthermalsci.2006.05.002.

[60] Bejan A. General criterion for rating heat-exchanger performance. Int J Heat Mass Transf 1978;21:655–8. https://doi.org/10.1016/0017-9310(78)90064-9.

[61] Iverson BD, Conboy TM, Pasch JJ, Kruizenga AM. Supercritical CO2 Brayton cycles for solar-thermal energy. Appl Energy 2013;111:957–70.

[62] Pasch J, Conboy T, Fleming D, Rochau G. Supercritical CO2 Recompression Brayton Cycle: Completed Assembly Description. SANDIA Rep 2012.

[63] Conboy T, Pasch J, Fleming D. Control of a Supercritical {CO}2Recompression Brayton Cycle Demonstration Loop. Vol. 8 Supercrit. {CO}2 Power Cycles$\mathsemicolon$ Wind Energy$\mathsemicolon$ Honor. Award., ASME; 2013. https://doi.org/10.1115/gt2013-94512.

[64] Milewski J, Badyda K, Miller A. Gas Turbines in Unconventional Applications. Effic. Perform. Robustness Gas Turbines, InTech; 2012. https://doi.org/10.5772/37321.